

HIGHER-ORDER ANTI-DERIVATIVES OF BAND LIMITED STEP FUNCTIONS FOR THE DESIGN OF RADIAL FILTERS IN SPHERICAL HARMONICS EXPANSIONS

Nara Hahn, Frank Schultz, and Sascha Spors

Institute of Communications Engineering
University of Rostock, Rostock, Germany
nara.hahn@uni-rostock.de

ABSTRACT

This paper presents a discrete-time model of the spherical harmonics expansion describing a sound field. The so-called radial functions are realized as digital filters, which characterize the spatial impulse responses of the individual harmonic orders. The filter coefficients are derived from the analytical expressions of the time-domain radial functions, which have a finite extent in time. Due to the varying degrees of discontinuities occurring at their edges, a time-domain sampling of the radial functions gives rise to aliasing. In order to reduce the aliasing distortion, the discontinuities are replaced with the higher-order anti-derivatives of a band-limited step function. The improved spectral accuracy is demonstrated by numerical evaluation. The proposed discrete-time sound field model is applicable in broadband applications such as spatial sound reproduction and active noise control.

1. INTRODUCTION

The spherical harmonics expansion represents a sound field as a linear combination of spherical harmonics weighted by the corresponding coefficients [1, 2]. It is widely used in applications such as sound field analysis using microphone arrays and spatial sound reproduction (e.g. Ambisonics) [3–5]. The radial and frequency dependent parts of the coefficients, called radial functions, are described by the spherical Bessel/Hankel functions. In broadband cases, a numerical simulation in the frequency domain is cumbersome since it requires the evaluation of special functions over a wide range of frequency bins. Moreover, the inverse discrete Fourier transform (IDFT) often suffers from long transients and temporal aliasing.

In order to overcome this problem, the broadband radial functions are implemented in the time domain as digital filters, called *radial filters*. For microphone and loudspeaker arrays baffled on a rigid sphere, the spatial impulse responses have infinite temporal extent. Therefore, the radial functions and also their inverse (equalization filters) are realized as infinite impulse response (IIR) filters [6–9]. For homogeneous sound fields, which will be considered in this paper, the spatial impulse responses exhibit a finite extent. The corresponding radial functions are thus modeled by finite impulse response (FIR) filters, whose coefficients are directly obtained from the analytical expressions of the time-domain sound field. This approach has been used in applications using loudspeaker arrays surrounding the listening area, e.g. wave fields synthesis and active noise control [10–12].

Copyright: © 2021 Nara Hahn et al. This is an open-access article distributed under the terms of the Creative Commons Attribution 3.0 Unported License, which permits unrestricted use, distribution, and reproduction in any medium, provided the original author and source are credited.

The design accuracy of the FIR-type radial filters is often limited by aliasing artifacts. This is mainly attributed to the discontinuities occurring in the time-domain radial functions, which exhibit an infinite bandwidth. Depending on the degree of the spectral distortion caused by aliasing, the perceived audio quality of the application may be impaired. Recently, the authors investigated how the spectral accuracy is influenced by different design parameters such as radius, harmonic order, and time shift [13, 14]. A radial filter design with reduced distortion was also presented, which is based on the anti-aliasing method that was introduced in [15–17]. The fundamental idea is to replace the discontinuities with smooth(er) transients. The 0th-order radial function (i.e. a rectangular pulse) is built by using the so-called band-limited step (BLEP) function, which is an integrated band-limited impulse (BLIM) [15, 18]. The coefficients of higher-order radial filters are then computed with the recurrence relation of the Legendre polynomials.

This paper presents an improved radial filter design, where the aliasing caused by the discontinuities in higher-order derivatives is addressed explicitly. To this end, the higher-order discontinuities occurring in the radial functions are examined (Sec. 2). The aliasing distortion is reduced by means of higher-order anti-derivatives of the BLEP functions (Sec. 3). Numerical simulations demonstrate the validity of the proposed method (Sec. 4), where the spectral accuracy of the radial filters is evaluated for varying anti-derivative orders. It is shown that the proposed radial filter design is more versatile compared with the conventional approach.

2. TIME-DOMAIN REPRESENTATION OF SPHERICAL HARMONICS EXPANSION

This section briefly reviews the spherical harmonics representation of a single plane wave. The more general cases of interior sound fields can be treated as a superposition of multiple plane waves [4, Sec. 2.4]. The position vector $\mathbf{x} = (x, y, z)^T$ is denoted by

$$\mathbf{x} = (r \sin \theta \cos \phi, r \sin \theta \sin \phi, r \cos \theta)^T \quad (1)$$

with $r \geq 0$, $\theta \in [0, \pi]$, $\phi \in [0, 2\pi)$ denoting the radius, colatitude, and azimuth, respectively. The propagating direction of the plane wave is described by the unit vector,

$$\mathbf{n}_p = (\sin \theta_p \cos \phi_p, \sin \theta_p \sin \phi_p, \cos \theta_p)^T, \quad (2)$$

where θ_p, ϕ_p denote the respective colatitude and azimuth angles.

The sound field of a harmonic plane wave can be represented

as an interior expansion [4, Eq. (2.38)],

$$\begin{aligned} e^{-i\frac{\omega}{c}\cos\Theta} &= \sum_{n=0}^{\infty} \sum_{m=-n}^n 4\pi i^{-n} j_n\left(\frac{\omega}{c}r\right) Y_{nm}^*(\theta_p, \phi_p) Y_{nm}(\theta, \phi) \\ &= \sum_{n=0}^{\infty} (2n+1) i^{-n} j_n\left(\frac{\omega}{c}r\right) P_n(\cos\Theta), \end{aligned} \quad (3)$$

where Θ denotes the angle between \mathbf{x} and \mathbf{n}_p . The time harmonic term $e^{i\omega t}$ is omitted for brevity. In the first equality, the angular dependency is described by the spherical harmonics $Y_{nm}(\cdot)$. The asterisk $(\cdot)^*$ denotes the complex conjugate. The addition theorem of the spherical harmonics is exploited in the second equality [19, Eq. (14.18.2)]. The axis-symmetry of the sound field with respect to \mathbf{n}_p leads to a simplified expression, where $P_n(\cdot)$ are the Legendre polynomials. Regardless of the spatial symmetry, the frequency and radial dependencies are described by the spherical Bessel functions of the first kind $j_n(\frac{\omega}{c}r)$ together with the phase term i^{-n} . These are called the frequency-domain radial functions ($n = 0, \dots, 3$) are depicted in Fig. 1.

The time-domain representation of a plane wave excited by a Dirac delta function $\delta(t)$ reads [19, Eq. (10.59.1)][20]

$$\delta\left(t - \frac{r}{c} \cos\Theta_p\right) = \frac{c}{2r} \sum_{n=0}^{\infty} (2n+1) \tilde{P}_n\left(\frac{c}{r}t\right) P_n(\cos\Theta_p), \quad (4)$$

where $\tilde{P}_n(\cdot)$ denotes Legendre polynomials windowed by a rectangular pulse such that

$$\tilde{P}_n(\nu) := \begin{cases} P_n(\nu), & |\nu| < 1 \\ \frac{1}{2}P_n(\nu), & |\nu| = 1 \\ 0, & |\nu| > 1. \end{cases} \quad (5)$$

As shown in Fig. 2 (top row), the time-domain radial functions coincide with the Legendre polynomials for $|\frac{c}{r}t| < 1$, and are zero elsewhere. The values at the jump discontinuities ($|\frac{c}{r}t| = 1$) are not uniquely defined [21, Sec. 9.6], as they have no effect on the Fourier transform relationship,

$$\mathcal{F}_t\left\{\frac{c}{2r}\tilde{P}_n\left(\frac{c}{r}t\right)\right\} = i^{-n}j_n\left(\frac{\omega}{c}r\right). \quad (6)$$

For the definition in (5), the mean value of the left and right limits are chosen for convenience (not shown in Fig. 2).

Due to their finite extent, it is reasonable to realize the time-domain radial functions as FIR filters in discrete-time domain. It is worth noting that there exist filter design methods that approximate a finite impulse response by using IIR filters [22, 23]. However, these approaches are beyond the scope of this paper and will not be considered in the remainder. Instead, FIR filters are designed by sampling the continuous-time representations of the radial functions. Without employing any countermeasure, the sampled radial functions inevitably suffer from aliasing distortion since the original spectrum is not strictly band limited (cf. Fig. 1). The aliasing artifacts occurring in discrete-time radial functions were investigated in [14], revealing the influence of radius, harmonic order, and fractional sample delay on the design accuracy.

The aliasing distortion is caused by the abrupt change of the function at $|\frac{c}{r}t| = 1$. This does not only apply to the jump discontinuities but also to the discontinuities of their higher-order derivatives,

$$\tilde{P}_n^{(k)}(\cdot) := \frac{d^k}{dt^k} \tilde{P}_n(\cdot), \quad (7)$$

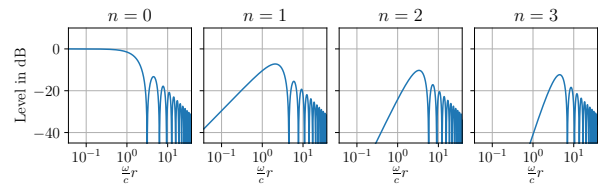


Figure 1: The magnitude of frequency-domain radial functions $i^{-n}j_n(\frac{\omega}{c}r)$.

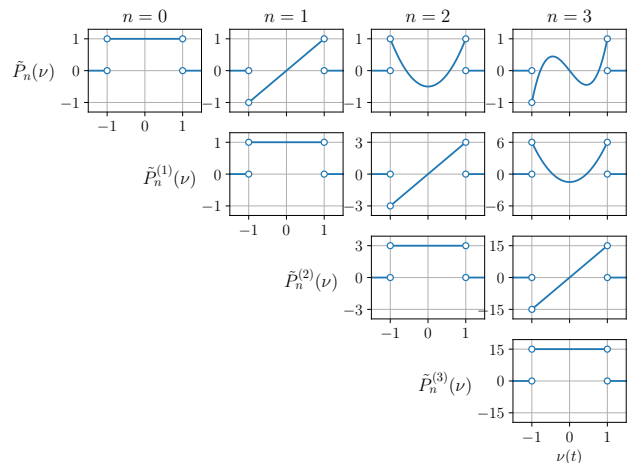


Figure 2: Time-domain radial functions (cf. (4), (5)) and their derivatives with respect to the argument. For brevity, the argument is normalized $\nu = \frac{c}{r}t$ and the scaling factor $\frac{c}{2r}$ is omitted. The values at $\nu = \pm 1$ are not shown. Note the different scale of the vertical axes.

such as slope ($k = 1$) and curvature ($k = 2$). The left and right limits of the derivatives are different at those points,

$$\lim_{\epsilon \rightarrow 0} \left[\tilde{P}_n^{(k)}(\pm 1 + \epsilon) - \tilde{P}_n^{(k)}(\pm 1 - \epsilon) \right] \neq 0. \quad (8)$$

The higher-order discontinuities can be examined by using the Taylor series expansion of the Legendre polynomials [19, Eq. (1.4.35)]. For convenience, a normalized argument $\nu = \frac{c}{r}t$ is used below. The series expansion at $\nu = 1$ reads

$$P_n(\nu) = \sum_{k=0}^{\infty} \frac{P_n^{(k)}(1)}{k!} (\nu - 1)^k. \quad (9)$$

The coefficients can be obtained by comparing (9) with an explicit expression of the Legendre polynomials [24, p. 1]

$$P_n(\nu) = \sum_{k=0}^n \binom{n}{k} \binom{n+k}{k} \left(\frac{\nu-1}{2}\right)^k \quad (10)$$

$$= \sum_{k=0}^n \frac{(n+k)!}{(n-k)! k! k! 2^k} (\nu-1)^k \quad (11)$$

$$= \sum_{k=0}^n \frac{\beta_n(k)}{k!} (\nu-1)^k \quad (12)$$

where $\binom{\cdot}{\cdot}$ denote the binomial coefficients and $\beta_n(k) = \frac{(n+k)!}{(n-k)!k!2^k}$ the coefficients of the Bessel polynomials [25, Eq. (3)]. The k th derivatives at $\nu = 1$ are therefore

$$P_n^{(k)}(1) = \begin{cases} \beta_n(k), & k = 0, \dots, n \\ 0, & k \geq n + 1. \end{cases} \quad (13)$$

Since $P_n(\nu)$ is an n th-order polynomial, derivatives of order higher than n are zero.

The Taylor series expansion with respect to $\nu = -1$ can be obtained by exploiting the reflection formula [19, Eq. (14.7.17)],

$$P_n(-\nu) = (-1)^n P_n(\nu), \quad (14)$$

from which it follows (using the chain rule)

$$(-1)^k P_n^{(k)}(-\nu) = (-1)^n P_n^{(k)}(\nu), \quad (15)$$

and in combination with (13) yields

$$P_n^{(k)}(-1) = \begin{cases} (-1)^{n-k} \beta_n(k), & k = 0, \dots, n \\ 0, & k \geq n + 1. \end{cases} \quad (16)$$

The corresponding Taylor expansion thus reads

$$P_n(\nu) = \sum_{k=0}^n (-1)^{n-k} \frac{\beta_n(k)}{k!} (\nu + 1)^k. \quad (17)$$

Based on (12) and (17), the higher-order discontinuities occurring in the windowed Legendre polynomials $\tilde{P}_n(\nu)$ can be examined. The changes of the k th coefficient at $\nu = \pm 1$ are

$$\hat{\eta}_n^k(1) = \lim_{\epsilon \rightarrow 0} \left[\frac{1}{k!} \tilde{P}_n^{(k)}(1 + \epsilon) - \frac{1}{k!} \tilde{P}_n^{(k)}(1 - \epsilon) \right] \quad (18)$$

$$= -\frac{\beta_n(k)}{k!} \quad (19)$$

and

$$\hat{\eta}_n^k(-1) = \lim_{\epsilon \rightarrow 0} \left[\frac{1}{k!} \tilde{P}_n^{(k)}(-1 + \epsilon) - \frac{1}{k!} \tilde{P}_n^{(k)}(-1 - \epsilon) \right] \quad (20)$$

$$= (-1)^{n-k} \frac{\beta_n(k)}{k!}, \quad (21)$$

respectively. The hat $\hat{\cdot}$ indicates that the derivatives are performed with respect to the normalized variable ν . Equation (19) and (21) exploit that

$$\tilde{P}_n^{(k)}(\nu) = 0, \quad (22)$$

for $|\nu| > 1$ and $k \in \mathbb{Z}_{\geq 0}$. The discontinuities of different derivative orders k are depicted in Fig. 2.

The actual discontinuities exhibited by the time-domain radial functions are obtained by re-scaling the argument,

$$\nu = \frac{c}{r} t, \quad \frac{d^k}{d\nu^k} = \left(\frac{r}{c}\right)^k \frac{d^k}{dt^k}, \quad (23)$$

and introducing the factor $\frac{c}{2r}$ from (4), yielding

$$\eta_n^k(1) = -\frac{1}{2k!} \left(\frac{c}{r}\right)^{k+1} \beta_n(k) \quad (24)$$

and

$$\eta_n^k(-1) = (-1)^{n-k} \frac{1}{2k!} \left(\frac{c}{r}\right)^{k+1} \beta_n(k). \quad (25)$$

Note that η_n^k is now without hat. The Bessel polynomial coefficients can be computed recursively,

$$\beta_n(k) = (2n - 1)\beta_{n-1}(k - 1) + \beta_{n-2}(k) \quad (26)$$

with $\beta_n(0) = 1$ and $\beta_1(1) = 1$ [25, Eq. (3) and (21)].

By using (24) and (25), the radial functions (4) can be expressed in terms of their higher-order discontinuities [20, Eq. (6)],

$$\begin{aligned} & \frac{c}{2r} \tilde{P}_n\left(\frac{c}{r}t\right) \\ &= \sum_{k=0}^n \left[\eta_n^k(-1) \left(t + \frac{r}{c}\right)^k u\left(t + \frac{r}{c}\right) + \eta_n^k(1) \left(t - \frac{r}{c}\right)^k u\left(t - \frac{r}{c}\right) \right] \\ &= \frac{c}{2r} \sum_{k=0}^n \frac{\beta_n(k)}{k!} \left(\frac{c}{r}\right)^k \\ & \quad \times \left[(-1)^{n-k} \left(t + \frac{r}{c}\right)^k u\left(t + \frac{r}{c}\right) - \left(t - \frac{r}{c}\right)^k u\left(t - \frac{r}{c}\right) \right], \end{aligned} \quad (27)$$

where $u(t)$ denotes the Heaviside step function. The time-domain radial functions thus can be represented as a superposition of two right-sided signals. The first one emerges at $t = -\frac{r}{c}$ and is canceled by the second one for $t > \frac{r}{c}$. The position of each discontinuity is explicitly known, which is beneficial for the band limitation method discussed in the following section.

3. HIGHER-ORDER ANTI-DERIVATIVES OF BAND LIMITED STEP FUNCTIONS

This section addresses the reduction of aliasing caused by sampling the higher-order discontinuities. An analytical low-pass filtering is applied to the continuous-time representation (27) so that the radial functions can be sampled with significantly reduced aliasing distortion. The employed method was initially introduced in [15] and has been extensively studied in the past decades [16, 17]. The treatment of second-order discontinuities was introduced in [26–28].

Higher-order discontinuities can be described by successive anti-derivatives of the Dirac delta function,

$$F_0(t) = \int_{-\infty}^t \delta(t') dt' = u(t) \quad (28)$$

$$F_k(t) = \int_{-\infty}^t F_{k-1}(t') dt' = \frac{t^k}{k!} \cdot u(t), \quad (29)$$

for $k \geq 1$. A low-pass filtered version of each discontinuity is obtained by replacing $\delta(t)$ with a low-pass filter $h(t)$,

$$H_0(t) = \int_{-\infty}^t h(t') dt' \quad (30)$$

$$H_k(t) = \int_{-\infty}^t H_{k-1}(t') dt', \quad (31)$$

for $k \geq 1$. In the literature, the low-pass filter $h(t)$ is commonly referred to as the band-limited impulse (BLIM), $H_0(t)$ the band-limited step (BLEP) function, and $H_1(t)$ the band-limited ramp (BLAMP) function [18, 27]. The prototype filter $h(t)$ is often linear phase but nonlinear-phase filters can be also used [29].

In this method, the discontinuities $F_k(t)$ are replaced with smooth transitions described by $H_k(t)$. The residual function,

$$D_k(t) = H_k(t) - F_k(t) = H_k(t) - \frac{t^k}{k!} u(t), \quad (32)$$

is appropriately delayed, scaled, and then added to the signal to be sampled. This leads to a low-pass filtered expression of the signal in the continuous-time domain. Since $H_k(t)$ and $D_k(t)$ correspond to a discontinuity of $\frac{1}{k!}t^k u(t)$, the scaling factor $\frac{1}{k!}$ should be accounted for.

The performance and efficiency of this method are affected by the choice of the BLIM. Although having ideal low-pass filter characteristics, the sinc function cannot be used in its original form because of the infinite temporal extent. Occasionally, a windowed sinc function is used as an approximation, which however lacks the computational efficiency due to the involved trigonometric functions. In practice, a BLIM is often built by using a polynomial interpolator [17]. This also suits the presented approach, as the higher-order anti-derivatives can be computed more efficiently.

In this paper, the impulse response of a Lagrange interpolator [30] is considered. For an M th-order interpolation, the BLIM is described by M th-order polynomials in $M+1$ adjacent intervals ($M+2$ nodes),

$$h(t) = \begin{cases} h_m(t), & \frac{t}{T} + \frac{M+1}{2} \in [m, m+1) \\ 0, & \text{elsewhere,} \end{cases} \quad (33)$$

for $m = 0, \dots, M+1$. The impulse response is even symmetric with respect to $t = 0$. Only odd M is considered since it is superior in terms of spectral properties [31]. An exemplary BLIM ($M = 5$) is depicted in Fig. 3 (left column). It is assumed that the intervals have the same length T , for which the spectrum exhibits zeros at angular frequencies $\omega = \mu \frac{2\pi}{T}$ with $\mu \in \mathbb{Z}$ [32, Sec. 5.3]. One half of the first zero frequency $\omega_c = 2\pi f_c = \frac{\pi}{T}$ is considered as the cut-off frequency of the low-pass filter $h(t)$. The bandwidth of the BLIM thus can be changed by varying T . For $T = T_s$, the corresponding bandwidth is half the sampling frequency $\frac{\omega_s}{2} = \pi f_s$.

The integration of the individual piecewise polynomials $h_m(t)$ in (33) is generally not continuous as illustrated in Fig. 3 (top row). In each interval, an integration constant has to be chosen in such a way that the anti-derivatives are continuous at the boundaries. The polynomials in the first and last interval have to satisfy

$$H_k(t - \frac{M+1}{2}T) = 0 \quad (34)$$

$$H_k(t + \frac{M+1}{2}T) = \frac{t^k}{k!}, \quad (35)$$

respectively for $k = 0, \dots, K$. These conditions can be fulfilled only for $K \leq M$, meaning that the maximum anti-derivative order K is limited by the BLIM order M . Figure 3 (middle row) shows the resulting functions. The residuals $D_k(t)$ are obtained by subtracting $\frac{1}{k!}t^k u(t)$ from $H_k(t)$ as depicted in Fig. 3 (bottom row). Figure 4 shows the residuals for different Lagrange polynomial orders M . The even order anti-derivative residual functions are odd symmetric and vice versa.

The frequency responses of the residual functions are depicted in Fig. 5. The radial functions exhibit zero(s) at DC, except for $k = M$ (—) where the spectrum resembles that of a low-pass filter. Anti-derivatives of order higher than M (not shown) will introduce poles(s) at DC, leading to unstable transfer functions. An integration in the time domain with respect to $\frac{t}{T}$ corresponds to a multiplication by $\frac{1}{i\omega T}$ in the frequency domain [21, Sec. 9.7.8]. The slope of the spectrum changes accordingly. The curves intersect with each other at $\frac{\omega}{\omega_c} = \frac{1}{\pi} \approx 0.318$ where the magnitude

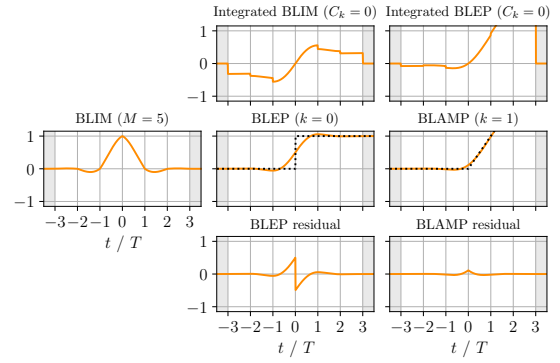


Figure 3: BLIM, BLEP and BLAMP functions (Lagrange polynomials $M = 5$). The dotted lines \cdots in the middle row indicate the unit step and ramp functions. The time extent of the piecewise polynomial is indicated by the white background.

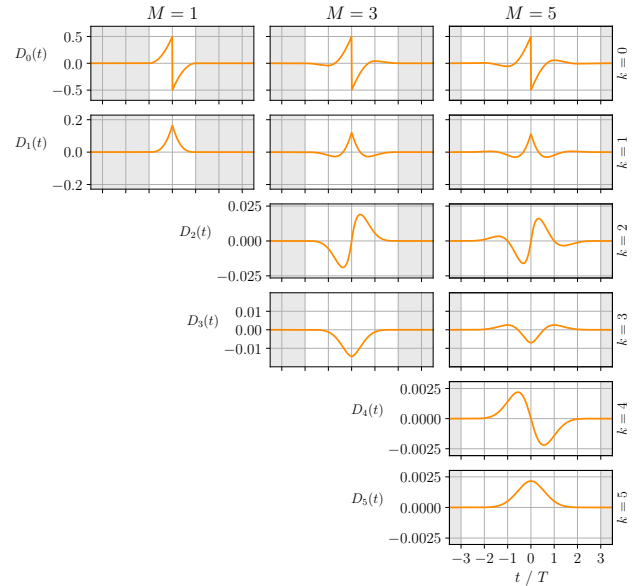


Figure 4: Residual functions $D_k(t)$ derived from Lagrange polynomials of different orders M . Note the different scale of the vertical axes for each k . The length of the residual is $(M+1) \cdot T$ as indicated by white background.

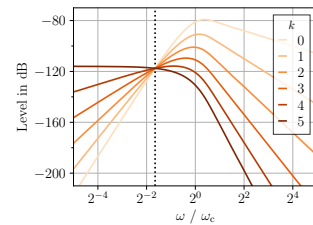


Figure 5: Spectra of the residual functions (Lagrange polynomial $M = 5$, cf. right column of Fig. 4). The frequency axis is normalized by $\omega_c = \frac{\pi}{T}$. The dotted line indicates $\frac{\omega}{\omega_c} = \frac{1}{\pi}$.

response does not change by integration, i.e.

$$\left| \frac{1}{i\omega T} \right| = \left| \frac{\omega_c}{i\pi\omega} \right| = 1. \quad (36)$$

This is indicated by the dotted line (....) in Fig. 5.

Finally, low-pass filtered expressions of the radial functions are yielded by introducing the band-limited discontinuities to (27),

$$\begin{aligned} & \frac{c}{2r} \tilde{P}_n\left(\frac{c}{r}t\right) *_t h(t) \\ &= \frac{c}{2r} \sum_{k=0}^K \beta_n(k) \left(\frac{c}{r}\right)^k \left((-1)^{n-k} H_k\left(t + \frac{r}{c}\right) - H_k\left(t - \frac{r}{c}\right) \right) \\ &= \frac{c}{2r} \tilde{P}_n\left(\frac{c}{r}t\right) + \frac{c}{2r} \sum_{k=0}^K \left[\beta_n(k) \left(\frac{c}{r}\right)^k \right. \\ & \quad \left. \times \left((-1)^{n-k} D_k\left(t + \frac{r}{c}\right) - D_k\left(t - \frac{r}{c}\right) \right) \right], \end{aligned} \quad (37)$$

where $K \leq \min(n, M)$. An additional condition for K with regard to n needs to be included as the discontinuity order of the radial function does not exceed n . Note that the term $\frac{1}{k!}$ from (27) is canceled. The above equation states that the convolution ($*_t$) of the radial functions with the BLIM $h(t)$ is equivalent to a superposition of the former with linearly combined residual functions $D_k(t \pm \frac{r}{c})$.

Since (37) is a continuous-time expression, it can be sampled at arbitrary points. In practice, the original radial functions (without band limitation) are first discretized and then the samples in the neighborhood of the discontinuities ($|\frac{c}{r}t| = 1$) are updated according to the residual functions. The number of modified samples per discontinuity is $\lfloor (M+1)\frac{T}{T_s} \rfloor$ with $\lfloor \cdot \rfloor$ denoting the floor function.

4. EVALUATION

In this section, radial filters are designed based on the band-limited expression (37), and their temporal and spectral properties are examined. All simulations are performed at a sampling frequency of $f_s = 48$ kHz. The radius is assumed to be $r = 1$ m and the speed of sound is set to $c = 343$ m/s.

Figure 6 shows the band-limited radial functions ($n = 0, \dots, 5$) that are built by using 5th-order Lagrange polynomials. For each n , the maximum anti-derivative order is $K = n$. In order to better visualize the transients around $|\frac{c}{r}t| = 1$, the polynomial interval is set to $T = \frac{48}{5} \cdot T_s = \frac{1}{5}$ ms ($f_c = 2.5$ kHz). The smooth shape of the radial functions is apparent. Slight under- and overshoots can be observed, which follow the impulse response of the Lagrange interpolator.

The spectral accuracy of discrete-time radial functions are examined in Fig. 7. The same parameters ($M = 5, K = n$) are considered as in Fig. 6, except for the interval $T = T_s$ ($f_c = \frac{f_s}{2} = 24$ kHz). The frequency responses (—) are computed by evaluating the discrete-time Fourier transform (DTFT) of the sampled radial functions and compared with the exact spectrum $i^{-n} j_n(\frac{\omega}{c}r)$ (■). The difference of the complex spectra are depicted (—). The radial functions are quite accurate up to 10 kHz, where the distortions stay below -80 dB. The spectrum of the radial functions roll off in the neighborhood of $\frac{f_s}{2}$, resulting in an increase of distortion. This is attributed to the spectral properties of the Lagrange

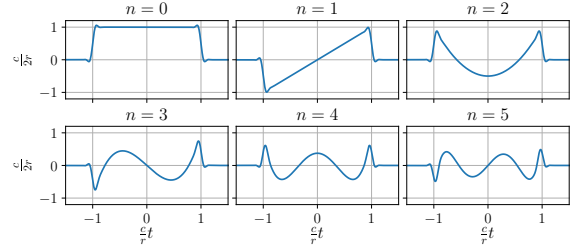


Figure 6: Band-limited radial functions ($r = 1$ m, $f_s = 48$ kHz, $T = \frac{48}{5} \cdot T_s = \frac{1}{5}$ ms, $M = 5, K = n$).

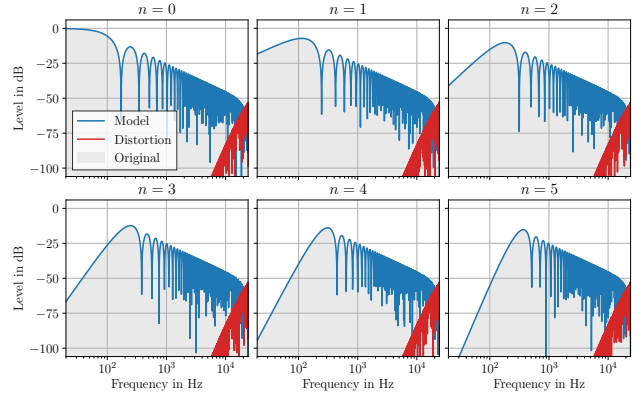


Figure 7: Frequency responses of the discrete-time radial filters (—) and the corresponding spectral distortions (—) ($r = 1$ m, $f_s = 48$ kHz, $T = T_s, M = 5, K = n$). The shaded area (■) indicates the exact frequency-domain radial functions $i^{-n} j_n(\frac{\omega}{c}r)$.

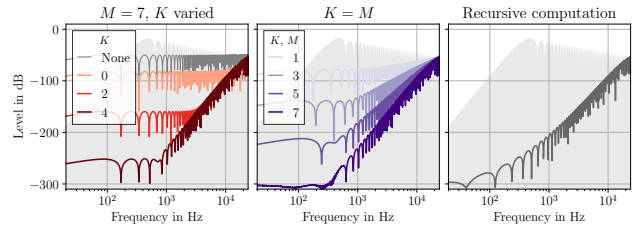


Figure 8: Spectral distortions of radial filters ($n = 7, r = 1$ m, ■: original spectrum). Left and Center: Using higher-order anti-derivatives of BLEP function. Right: Using BLEP function ($M = 7$) and the recurrence relation of the Legendre polynomials (38).

interpolation, which deviates from an ideal low-pass filter at high frequencies [30, 31].

The influence of the anti-derivative order is illustrated in Fig. 8 (left), where $n = 7$ and $M = 7$. The maximum anti-derivative order is varied $K = 0, 2, 4$. The thin curve (— labeled 'None') indicates the aliasing distortion if the radial function (27) is sampled without any treatment for anti-aliasing. The improvement achieved by smoothing the higher-order discontinuities is clearly seen. Notice that the aliasing at high frequencies is mostly reduced by lower-order anti-derivatives (e.g. $K = 2$). The residual functions of higher orders have little effect around $\frac{f_s}{2}$, but improve the accuracy in low frequencies. Considering that the radial functions

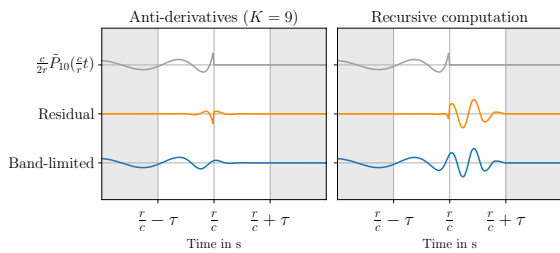


Figure 9: Tenth-order radial function ($r = 1$ m, $M = 9$, $f_s = 48$ kHz, $T = \frac{48}{5} \cdot T_s$, $\tau = \frac{M+1}{2} T$). Left: Using higher-order anti-derivatives of BLEP function ($K = 9$). Right: Using BLEP function and the recurrence relation (38).

($n \geq 1$) have a DC null in their spectrum (cf. Fig. 1), higher-order anti-derivatives are crucial for a high signal-to-aliasing ratio in low frequencies.

In Fig. 8 (center), the same radial function ($n = 7$) is modeled with varying Lagrange polynomial orders $M = 1, 3, 5, 7$. The number of modified samples around the discontinuities varies accordingly. The maximum anti-derivative order is set equal to the polynomial order $K = M$. As M increases, the decay of the spectral distortion around $\frac{f_s}{2}$ gets steeper due to the increasing slope of the Lagrange interpolator [31].

The result of the conventional method used in [13, 14] is depicted in Fig. 8 (right \rightarrow). The 0th-order radial function, which has only 1st-order discontinuities (cf. Fig. 2), is designed by using the BLEP residuals (Lagrange $M = 7$). Higher-order radial functions are computed by exploiting the recurrence relation of the Legendre polynomials [19, Eq. (14.10.3)],

$$n P_n\left(\frac{c}{r}t\right) = (2n - 1)\left(\frac{c}{r}t\right)P_{n-1}\left(\frac{c}{r}t\right) - (n - 2)P_{n-2}\left(\frac{c}{r}t\right). \quad (38)$$

In terms of spectral distortion, the result is slightly inferior to the proposed method (shown in Fig 8 \rightarrow). Varying T leads to temporal artifacts as shown in Fig. 9 (right). As T increases (i.e. narrowing bandwidth), the sample values for $|\frac{c}{r}t| > 1$ are progressively amplified due to the factor $\frac{c}{r}t$ in the recurrence relation (38). The artifact becomes more prominent for higher spherical harmonic orders n . The approach proposed in this paper, on the other hand, is free from such oscillatory behavior as depicted in Fig. 9 (left).

5. DISCUSSION AND CONCLUSION

The radial and frequency dependent terms in the spherical harmonics expansions (i.e. the radial functions) are realized as digital filters. The FIR coefficients are derived from the analytical expressions of the time-domain radial functions. A band limitation is applied to the higher-order discontinuities occurring in the time-domain by using the higher-order anti-derivatives of the BLEP functions. This enables a time-domain sampling with considerably reduced aliasing distortion. Since the filter coefficients are expressed by polynomials (with argument of physical variables), the filters can be adapted instantaneously in response to parameter changes like source/receiver movements. The presented approach is expected to facilitate the development of broadband signal processing techniques that are based on spherical harmonics representations.

The band limitation approach employed in this paper has been commonly used in different contexts, e.g. for the digital emulation

of analog synthesizers [15–17] and aliasing-free modeling of nonlinear systems [26–28]. The radial filter design problem has some distinct aspects that are listed below.

- In other applications mentioned above, the considered signals typically have a line spectrum with harmonic structure. The perceived sound quality is directly affected by the inharmonic components caused by aliasing. Presumably, the B-spline interpolation is preferred because of its steeper high-frequency roll-off, which suppresses the aliasing more effectively at the expense of higher overtones. Contrarily, the radial filters are not intended for direct listening. Considering the insensitivity of human hearing to high-frequency phase differences, it seems reasonable to aim for a correct magnitude response while tolerating some phase distortion at high frequencies. In that regard, the Lagrange interpolator is a more suitable choice here. The audibility of the magnitude and phase distortion has to be further investigated by perceptual evaluations though.
- The radial functions exhibit different orders of discontinuities, all of which occur simultaneously. The maximum discontinuity order considered in this paper is higher than in other publications. The analysis in Sec. 4 demonstrates that the higher-order anti-derivatives of BLEP function are beneficial for reducing the aliasing in mid-to-low frequencies.
- In some applications, the point of jump discontinuity or the point of clipping has to be estimated in the sub-sample level. Fortunately, this is not of a concern in the presented filter design, as the explicit expressions for the radial functions are known.

In this paper, the band-limitation of higher-order discontinuities is addressed in a generalized scheme. The presented work thus can be also applied to different types of signals and systems with varying degrees of discontinuities.

6. REFERENCES

- [1] E. Williams, *Fourier Acoustics: Sound Radiation and Nearfield Acoustical Holography*. Academic Press, 1999.
- [2] N. A. Gumerov and R. Duraiswami, *Fast Multipole Methods for the Helmholtz Equation in Three Dimensions*. Elsevier, 2005.
- [3] J. Ahrens, *Analytic Methods of Sound Field Synthesis*. Springer, 2012.
- [4] B. Rafaely, *Fundamentals of Spherical Array Processing*, 2nd ed. Springer, 2019.
- [5] F. Zotter and M. Frank, *Ambisonics*. Springer, 2019.
- [6] H. Pomberger, “Angular and radial directivity control for spherical loudspeaker arrays,” Master’s thesis, University of Music and Performing Arts, Graz, Austria, 2008.
- [7] F. Zotter, “Analysis and synthesis of sound-radiation with spherical arrays,” Ph.D. dissertation, University of Music and Performing Arts, Graz, Austria, 2009.
- [8] S. Lösler and F. Zotter, “Comprehensive radial filter design for practical higher-order Ambisonic recording,” in *Proc. 41st German Annu. Conf. Acoust. (DAGA)*, 2015, pp. 452–455.

- [9] N. Hahn, F. Schultz, and S. Spors, “Spatio-temporal properties of simulated impulse responses on a rigid sphere,” in *Proc. 47th German Annu. Conf. Acoust. (DAGA)*, Wien, Austria, Aug. 2021, to be published.
- [10] M. Poletti, T. D. Abhayapala, and P. D. Teal, “Time domain description of spatial modes of 2D and 3D free-space Greens functions,” in *Proc. Audio Eng. Soc. (AES) Conf.*, Guildford, UK, 2016.
- [11] F. Ma, W. Zhang, and T. D. Abhayapala, “Reference signal generation for broadband ANC systems in reverberant rooms,” in *IEEE Int. Conf. Acoust. Speech Signal Process. (ICASSP)*, Calgary, Canada, 2018, pp. 216–220.
- [12] N. Hahn, F. Winter, and S. Spors, “2.5D local wave field synthesis of a virtual plane wave using a time domain representation of spherical harmonics expansion,” in *Proc. 23rd Int. Cong. Acoust. (ICA)*, Aachen, Germany, Sep. 2019, pp. 1132–1139.
- [13] N. Hahn and S. Spors, “Discrete time modeling of spherical harmonics expansion by using band-limited step functions,” in *Proc. 46th German Annu. Conf. Acoust. (DAGA)*, Hannover, Germany, Mar. 2020, pp. 1188–1191.
- [14] N. Hahn, F. Schultz, and S. Spors, “Time domain sampling of the radial functions in spherical harmonics expansions,” *IEEE Trans. Signal Process.*, to be published, doi: 10.1109/TSP.2021.3092892.
- [15] T. Stilson and J. O. Smith, “Alias-free digital synthesis of classic analog waveforms,” in *Proc. Int. Comput. Music Conf.*, Hong Kong, Aug. 1996.
- [16] V. Välimäki and A. Huovilainen, “Antialiasing oscillators in subtractive synthesis,” *IEEE Signal Process. Mag.*, vol. 24, no. 2, pp. 116–125, 2007.
- [17] V. Välimäki, J. Pekonen, and J. Nam, “Perceptually informed synthesis of bandlimited classical waveforms using integrated polynomial interpolation,” *J. Acoust. Soc. Am.*, vol. 131, no. 1, pp. 974–986, 2012.
- [18] E. Brandt, “Hard sync without aliasing,” in *Proc. Int. Computer Music Conf.*, Havana, Cuba, 2001, pp. 365–368.
- [19] F. W. J. Olver, D. W. Lozier, R. F. Boisvert, and C. W. Clark, *NIST Handbook of Mathematical Functions Handbook*. Cambridge University Press, 2010.
- [20] N. Hahn and S. Spors, “Time-domain representations of a plane wave with spatial band-limitation in the spherical harmonics domain,” in *Proc. 45th German Annu. Conf. Acoust. (DAGA)*, Rostock, Germany, Mar. 2019, pp. 1434–1439.
- [21] B. Girod, R. Rabenstein, and A. Stenger, *Signals and Systems*. Wiley, 2001.
- [22] T. Saramaki and A. T. Fam, “Properties and structures of linear-phase FIR filters based on switching and resetting of IIR filters,” in *IEEE Int. Symp. Circuits Syst.*, New Orleans, LA, USA, 1990, pp. 3271–3274.
- [23] A. Wang and J. O. Smith, “On fast FIR filters implemented as tail-canceling IIR filters,” *IEEE Trans. Signal Process.*, vol. 45, no. 6, pp. 1415–1427, 1997.
- [24] W. Koepf, *Hypergeometric Summation*. Springer, 1998.
- [25] H. L. Krall and O. Frink, “A new class of orthogonal polynomials: The Bessel polynomials,” *Trans. Am. Math. Soc.*, vol. 65, no. 1, pp. 100–115, 1949.
- [26] F. Esqueda, V. Välimäki, and S. Bilbao, “Rounding corners with BLAMP,” in *Proc. Int. Conf. Digit. Audio Effects (DAFx)*, Brno, Czech Republic, 2016, pp. 121–128.
- [27] ———, “Antialiased soft clipping using an integrated bandlimited ramp,” in *Proc. 24th Eur. Signal Process. Conf. (EUSIPCO)*, Budapest, Hungary, 2016, pp. 1043–1047.
- [28] F. Esqueda, S. Bilbao, and V. Välimäki, “Aliasing reduction in clipped signals,” *IEEE Trans. Signal Process.*, vol. 64, no. 20, pp. 5255–5267, 2016.
- [29] J. Pekonen and M. Holters, “Nonlinear-phase basis functions in quasi-bandlimited oscillator algorithms,” in *Proc. Int. Conf. Digit. Audio Effects (DAFx)*, York, UK, 2012, pp. 261–268.
- [30] T. I. Laakso, V. Välimäki, M. Karjalainen, and U. K. Laine, “Splitting the unit delay,” *IEEE Signal Process. Mag.*, vol. 13, no. 1, pp. 30–60, 1996.
- [31] A. Franck and K. Brandenburg, “A closed-form description for the continuous frequency response of Lagrange interpolators,” *IEEE Sig. Process. Lett.*, vol. 16, no. 7, pp. 612–615, 2009.
- [32] A. Franck, “Efficient algorithms for arbitrary sample rate conversion with application to wave field synthesis,” Ph.D. dissertation, Ilmenau University of Technology, 2012.